Biosensors and Bioelectronics 183 (2021) 113205

Contents lists available at ScienceDirect

Biosensors and Bioelectronics

journal homepage: http://www.elsevier.com/locate/bios

Rapid electrochemical biosensor for sensitive profiling of exosomal microRNA based on multifunctional DNA tetrahedron assisted catalytic hairpin assembly

Ye Zhang [a,b,1], Xiaohe Zhang [a,b,1], Bo Situ [a,b], Yuan Wu [a,d], Shihua Luo [a,b], Lei Zheng [a,b,**], Yurong Qiu [a,c,*]

[a] Department of Laboratory Medicine, Nanfang Hospital, Southern Medical University, Guangzhou, 510515, PR China
[b] Guangdong Engineering and Technology Research Center for Rapid Diagnostic Biosensors, Nanfang Hospital, Southern Medical University, Guangzhou, 510515, PR China
[c] Huayin Medical Laboratory Center Co., Ltd., Guangzhou, 510515, PR China
[d] School of Basic Medicine, Guangdong Medical University, Dongguan, 523808, PR China

ARTICLE INFO

Keywords:
Electrochemical biosensor
Profiling
Exosomal microRNA
Multifunctional DNA tetrahedron
Catalytic hairpin assembly

ABSTRACT

Profiling of exosomal microRNA (exo-miRNA) is very important for cancer diagnosis and treatment. However, rapid and sensitive determination the trace of exo-miRNA in clinical samples has not been developed. Herein, a robust electrochemical biosensor was proposed using multifunctional DNA tetrahedrons assisted catalytic hairpin assembly (MDTs-CHA) for exo-miRNA analysis. The MDTs-CHA, contained two multifunctional tetrahedrons (T1 and T2), leverage localized reaction and cascade amplification to enable rapid and ultrasensitive exo-miRNA analysis. Employing the MDTs-CHA, the electrochemical platform allowed quantitative measurement of exo-miRNA down to 7.2 aM in 30 min with good specificity. Furthermore, by profiling four tumor-associated exo-miRNAs (miR-1246, miR-221, miR-375, and miR-21) in a breast cancer cohort, this platform showed high efficiency (AUC: 0.989) and high sensitivity of 90.5% for breast tumors diagnoses, with 80% sensitivity for early diagnoses (stage I-IIa). Therefore, this platform has great potential in bioanalysis and clinical diagnostics.

1. Introduction

Exosomes are small extracellular vesicles (30–200 nm) which contained a variety of miRNAs, proteins, and DNA and other substances (Kalluri 2016; Kalluri and LeBleu 2020; Théry et al., 2002). By secreting exosomes, cells transport these substances to target cells, affecting the biological activity of target cells (Imjeti and Menck 2017; Ratajczak et al., 2006; Valadi et al., 2007). Numerous studies have proved that high levels of exo-miRNAs are found released by diverse tumor cell related to cancer metastasis (Yan et al., 2018; Zeng et al., 2018). Compared with the free miRNAs, exo-miRNAs are more stable due to the protection of exosomal membrane (Gao et al., 2019). Hence, the determination of exo-miRNAs holds great potential for early tumor diagnosis. At present, quantitative reverse transcription polymerase chain reaction (qRT-PCR) as "gold standard" approach for exo-miRNAs detection still suffers some defects, including time-consuming, expensive apparatus, and false positive (Reese et al., 2020; Tavallaie et al., 2018). Thus, it is necessary to propose new method with high sensitivity and specificity for exo-miRNAs analysis.

Recently, various methods have been developed for exo-miRNAs detection, such as nanomaterials (Lee et al., 2019; Pang et al., 2019), enzyme-assisted isothermal amplification (Li et al., 2020c; Tang et al., 2020; Wang et al., 2020), spherical nucleic acid (Liu et al., 2019) and so on. Despite their remarkable performances, these methods are not rapid and simple enough for easy-to-use exo-miRNAs analysis due to complex operation and strict reaction conditions. Accordingly, enzyme-free

* Corresponding author. Department of Laboratory Medicine, Nanfang Hospital, Southern Medical University, Guangzhou, 510515, Guangdong Province, PR China.
** Corresponding author. Department of Laboratory Medicine, Nanfang Hospital, Southern Medical University, Guangzhou, 510515, Guangdong Province, PR China.
E-mail addresses: nfyyzhenglei@smu.edu.cn (L. Zheng), qyr@smu.edu.cn (Y. Qiu).
[1] These authors contributed equally to this work.

https://doi.org/10.1016/j.bios.2021.113205
Received 3 December 2020; Received in revised form 17 March 2021; Accepted 24 March 2021
Available online 29 March 2021

strategies, including catalytic hairpin assembly (CHA) (Chen et al., 2019; Li et al., 2020a; Shen et al., 2020), hybridization chain reaction (HCR) (Liao et al., 2021; Miao and Tang 2020; Miti et al., 2020), and entropy-driven amplification circuits (EDC) (Li et al., 2019), have been exploited because of high specificity, easy to use, and high stability. However, the low sensitivity and inefficiency compromised the analysis capability of enzyme-free amplification-based biosensor.

To improve the sensitivity and efficiency of enzyme-free amplification-based biosensor, cascade amplification and localized reaction were adopted (Liu et al., 2020; Ning et al., 2020; Zhang et al., 2020b). For example, Zhu et al. designed a cascade amplification strategy by concatenating CHA and hyper-Branched HCR for RNA detection (Chu and Deng 2019). Yang et al. developed a cascade amplification based on duplex-specific nuclease and catalytic hairpin assembly strategy for miRNA detection (Zhu et al., 2020). Although the cascade amplification improves the detection sensitivity, these methods may confront with some defects: i) multiple reaction steps of cascade amplification results in time-consuming and tedious operation; ii) time-consuming reaction of cascade enzyme-free amplification and strict reaction conditions of enzyme-assist cascade amplification limit their clinical applications. iii) the leakage can be more serious because of incompatible reaction conditions.

DNA tetrahedron (DT), as an outstanding DNA nanoarchitecture may anchor user-defined mode of electroactive molecule owe to high addressability and controllability (Ozhalici-Unal and Armitage 2009; Wang and Chai 2020; Zhang et al., 2020b). It provides diverse amplified signal tags by chemical modification and DNA self-assembly. In addition, multiple DNA scaffolds can be provided by DT for loading reaction system, which could greatly increase the local concentration, so as to improve the efficiency of enzyme-free amplification. For example, Fan et al. designed a nucleic acid signal amplifiers using horseradish peroxidase-labeled tetrahedron for biosensing (Lin et al., 2014). Wang et al. designed a tetrahedron with multiple DNA scaffolds to improve the efficiency of hybridization chain reaction (Wang et al., 2019). To sum up, DT hold great value as an accelerator and transducer by its programmability and high loading capacity.

To address the disadvantages of cascade amplification and further improve the sensitivity for exo-miRNA detection, a rapid and ultrasensitive electrochemical platform was developed based on multifunctional DNA tetrahedrons assisted catalytic hairpin assembly (MDTs-CHA). Compare with the Huang's group work (Huang et al., 2020), our DNA tetrahedrons have multiple functions. Firstly, it is used to increase the local concentrations of CHA substrates by confining hairpins in a compact space, which greatly improve the reaction efficiency. Secondly, the DTs are designed for circular cascade, which obtain polynomial or exponential amplification. Thirdly, it provides stable and large area for loading electroactive molecule. As showed in Scheme 1, DTs (T1 and T2) were assembled first by one-step annealing process to ensure sufficient hybridization of DNA hairpins. In the presence of target exo-miRNA, the CHA on the DT1 was quickly initiated and large amount of blocked P strands were exposed, which led to the DT1 seized by the capture probe specifically. Then, the I1 strands on the DT1 could trigger the CHA on the DT2. Blocked P strands on DT2 were unfolded and captured by electrode. In a similar way, I2 strands on the DT2 could initiate T1 CHA. Consequently, plentiful DNA tetrahedrons were immobilized on the electrode surface for binding RuHex to generate an amplified electrochemical signal. Therefore, we can realize ultrasensitive detection in a short time owing to ingenious design of MDTs. The proposed method holds great promising perspective for profiling exo-miRNA.

2. Experiment section

2.1. Reagents and instruments

DL2000DNA Marker, 20 bp DNA ladder and agarose were purchased from TakaRa Biotech (Dalian, China). TE buffer was obtained from Biosharp (Anhui, China). Phosphate buffered saline (PBS) was acquired from Thermo Fisher Scientific Inc. (Shanghai, China). Tris-HCl buffer used as washing buffer with concentration of 10 mM Tris, 100 mM NaCl and 5 mM $MgCl_2$ (pH 7.4). TNaK hybridization buffer (pH 7.5) consisted of 125 mM NaCl, 20 mM Tris-HCl, and 20 mM KCl. Binding buffer for DTs assembly was PBS contained 0.55 mM $MgCl_2$. DNA oligonucleotides synthesized from Sangon Inc (Shanghai, China) are HPLC-purified (Table S1).

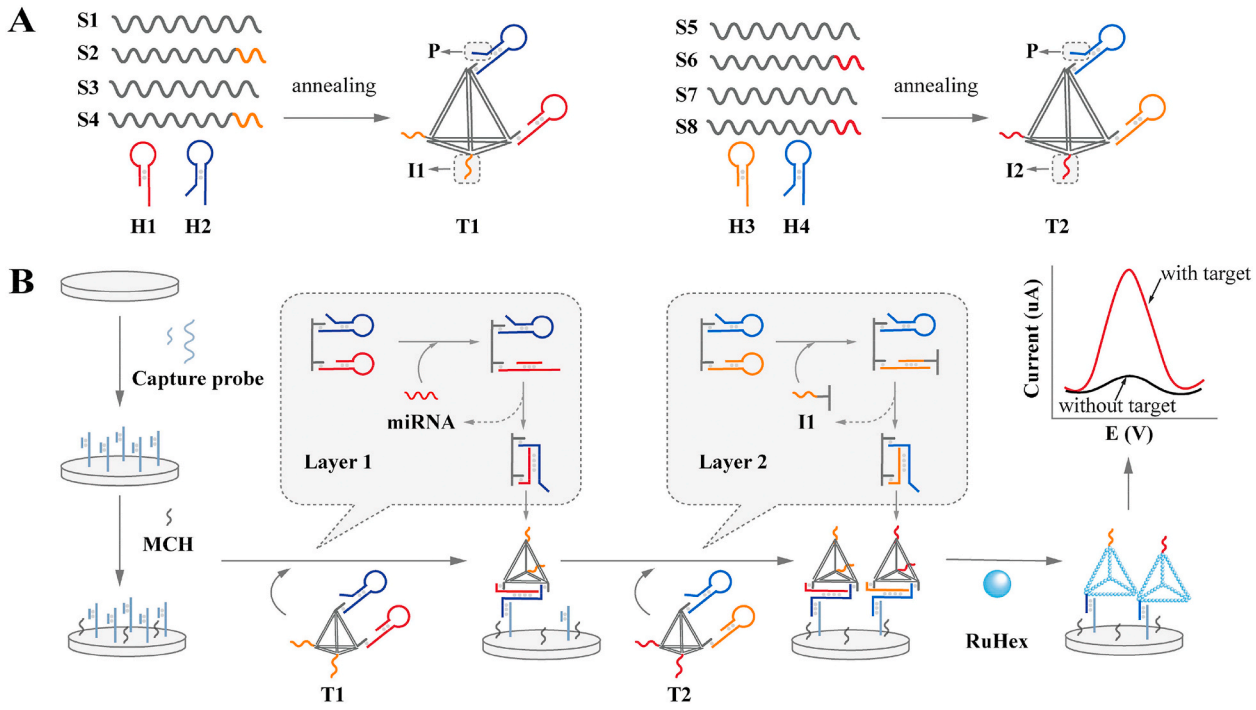

Scheme 1. Schematic representation of the electrochemical platform for exo-miRNA detection. (A) Assembly procedure of MDTs. (B) The operation steps of the two-layer MDTs-CHA.

Electrochemical measurements were performed on CHI660E electrochemical workstation (Shanghai Chenhua Instruments Co. Ltd., China), including impedance spectroscopy (EIS), square wave voltammetry (SWV), cyclic voltammetry (CV) and differential pulse voltammetry (DPV). The gel electrophoresis was conducted on a Syngene electrophoresis analyzer (Syngene, England). The ultracentrifuge was carried out with Beckman Optima XPN-100 (Beckman,USA). RT-qPCR was implemented and analyzed with Light Cycler 480 II (Roche, USA).

2.2. Preparation of DTs and CHA

The eight working probes (S1–S4, S5–S8) for assembling two MDTs were designed based on previous research, which synthesized DTs in one-step annealing. Hairpin probe 1 (H1), hairpin probe 2 (H2), hairpin probe 3 (H3) and hairpin probe 4 (H4) were designed obeyed the enzyme-free strand displacement reaction theory. All DNA oligonucleotides were denatured by the procedure of 95 °C lasting 5 min and lowered gradually to room temperature. The probes were stored at −20 °C for follow-up use. The two CHA amplification systems were mixture of two single-step synthesized TDNs and different hairpins in TNaK buffer, respectively. The MDTs-CHA reaction proceed rapidly with room temperature after adding target exo-miRNA. The double-strand capture probe was adopted, which could greatly decrease the background by inhibiting the breath reaction (Zhang et al., 2018).

The 2% agarose gels were prepared to confirm the synthesis of MDTs and products of CHA reaction. The 2% agarose gel electrophoresis was carried out in 1 × TAE buffer with 140 V constant voltage for 40 min. The gels were imagined and analyzed using Syngene G:BOX F3 Imaging System (Syngene, England).

2.3. Fluorescence measurements

The MDT-CHA amplification system with volume of 60 μL was measured by fluorescence signal. Luminescence Spectrometer (PerkinElmer LS-55, USA) was used for Fluorescence measurements (excitation wavelength of 488 nm; emission wavelength of 515 nm). The fluorescence intensity was recorded every 3 min for 30 min.

2.4. Preparation and measurement of electrochemical biosensor

The gold electrode was polished with 0.05 alumina powder, and then ultrasonically cleaned in deionized water for several times to remove residual alumina slurries. Next, the gold electrode was rinsed thoroughly with deionized water and allowed to dry at room temperature after soaking in piranha solution. 10 μL of 200 nM thiolated capture probe was dropped and incubated on the surface of gold electrode. After incubation overnight in 4 °C, 1 mM MCH was used for blocking the left bare sites of gold electrode.

MDTs-CHA amplification system consisted of DTs (T1 and T2), hairpin probes (H1 and H2; H3 and H4) and TNaK buffer. The final concentration of reaction substrates were 25 nM. 10 μL reaction mixture of MDTs-CHA and exo-miRNA was added on the electrode surface for 15 min. Following washed by Tris-HCl buffer, another CHA mixture including T2 was incubated with above MDTs-CHA products. The free substrates were rinsed by washing buffer. The DPV measurement was performed by immersing in Tris-HCl buffer containing 5 μM RuHex. All the treatments were carried out at 25 °C.

2.5. Isolation and RNA extraction of exosomes

Standard of procedure on plasma collection, handling, and storage was established in this study. Clinical plasma samples were collected from healthy donors and patients with breast tumor (Nanfang Hospital, Southern Medical University). All relevant operations were authorized by the Ethics Committee. The diagnoses were confirmed by histological examination of tissue biopsy. The serum samples (1 mL) were diluted to 2 mL with precooled-PBS and centrifuged at 3000×*g* for 20 min, 12,000×*g* for 45 min respectively. The cleared serum was separated and continued to centrifuge at 35,000 rpm for 15 min. Supernatants were completely removed, and repeated the above centrifugation step. Finally, exosomes were resuspended in 100 μL PBS. Transmission electron microscope (TEM) and nanoparticle tracking analysis (NTA) were used for exosomes characterizations.

Exosomal total RNAs were extracted by using Hipure Serum/Plasma miRNA Mini Kit (Magen, R4314-03). The quantification and quality of total RNA was evaluated by measuring the absorbance ratio at 260, 230 and 280 nm with Nanodrop 2000C (Thermo Fisher Scientific, USA). The obtained RNA products were stored at −80 °C for further use.

2.6. RT-PCR analysis

The Bulge-LoopTM miRNA qRT-PCR Starter Kit (Ribo, China) was employed to synthesize cDNA. The reverse transcription reactions were performed at 42 °C for 60 min, followed by 70 °C for 10 min. Subsequently, PCR was carried out on Light Cycler 480 II (Roche, USA) with U6 snRNA as internal reference according to the recommended operation. The incubation steps were as follows: 95 °C (10 min), 40 cycles of 95 °C (2 s), 60 °C (20 s), and 70 °C (10 s). The threshold cycle results were obtained from LightCycle software.

3. Results and discussion

3.1. Design principle of the electrochemical biosensor

The principle of the proposed platform is illustrated in Scheme 1. Exo-miR-1246 was chosen as model molecule due to highly expressed in breast tumor exosomes. The MDTs-CHA consisted of two DTs. Each DT includes four DNA strands (S1–S4; S5–S8). The free parts of two strands in DTs were used to hybridize with CHA system (H1 and H2; H3 and H4) (Scheme 1A). The T1 consisted of red regions (I1), which could initiate CHA on the T2. The T2 consisted of dull-red regions (I2), which could trigger CHA on the T1. The sticky end P in H2 and H4 strands, which could be hybridized with the capture probe on the surface of electrode by toe-hold mediated stand displacement, was blocked at first. In the presence of the target exo-miRNA, the H1–H2 assembly on the T1 was triggered by toehold strand displacement to expose sticky end P. Next, the T1 was seized by the capture probe, initiating H3–H4 assembly on the T2 by the I1 of T1. Then, the exposed sticky end P on the T2 bound to the surface of electrode. With the end of the two-layer MDTs-CHA cascade amplification, the DTs trapped on the surface of electrode were used to bind the electroactive substance RuHex by electrostatic interactions, achieving an amplified electrochemical signal for quantifiable detection of exo-miRNA (Scheme 1B).

3.2. Characterization and feasibility of the MDTs-CHA

The length of DT sides plays an important role in the CHA breath reaction, which led to background leakage. To investigate the effects of side length on the localized CHA, we designed three tetrahedrons with length side of 13, 17 and 26 base pairs (13-DT, 17-DT, 26-DT), respectively (Fig. 1A). The effects of side length were analyzed by DPV tests. As showed in Fig. 1B, the 17-DTs hold the high efficiency of CHA with S/B of 6.94, which had little effect on the background signal. On the contrary, the high background leakage of 13-DT and low efficiency of 27-DT did not improve the signal-to-noise ratio. Thus, 17-DT was chosen as the best DT for MDTs-CHA design.

The successful formation of the MDTs-CHA was also characterized by AFM (Fig. S1) and agarose gel electrophoresis. As shown in Fig. 1C, the sequences were combined into T1 (lines 1 to 4) in the form of two strands (S1 + S2), three strands (S1 + S2 + S3), 17-DTs (S1 + S2 + S3 + S4), and complete MDTs-CHA (S1 + S2 + S3 + S4+ H1+ H2). In addition, after the addition of target miRNA, more complex spatial

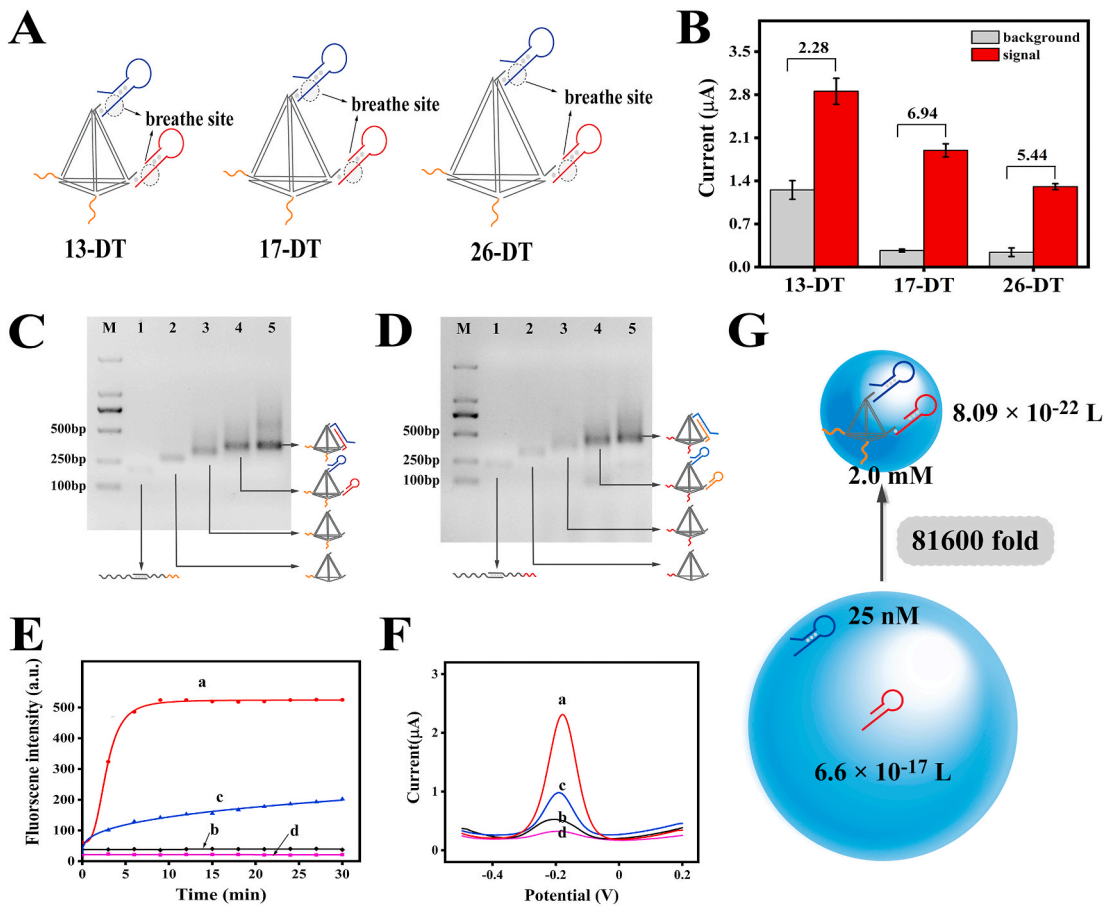

Fig. 1. (A) The breath sites in three tetrahedrons with length side of 13, 17 and 26 base pairs (13-DT, 17-DT, 26-DT). (B) Signal-to-background ratio for three different DT-CHA with target concentration of 100 pM. (C) 17-DT1 and (D) 17-DT2 assembly were analyzed using 2% agarose gel. Lane M, DNA ladder; lane 1, two strands (S1 + S2; S5 + S6); lane 2, three strands (S1 + S2 + S3; S5 + S6 +S7); lane 3, DNA tetrahedrons (S1 + S2 + S3 + S4; S5 + S6 + S7 + S8); lane 4, complete MDTs-CHA (DT1; DT2); Lane 5, MDTs-CHA with trigger (DT1-CHA with target miRNA; DT2-CHA with I1). (E) Fluorescence and (F) DPV measurements of MDTs-CHA and traditional CHA. (a), MDTs-CHA with target; (b), without target; (c), traditional CHA with target; (d), without target. (G) The concentrations and regions of MDTs-CHA and traditional CHA system. The error bars are the standard deviations by three repetitive assays (n = 3).

structure was formed, which led to the reduction of electrophoretic mobility (line 5). T2 was constructed in similar way (Fig. 1D), and complex spatial structure was formed in the presence of I1 (line 5). These results proved the successful assembly of the MDTs-CHA and exhibited the validity of detecting miRNAs.

The superiority of MDTs-CHA was demonstrated by DPV signal (Fig. 1F). Compared with conventional CHA, the significant signal and improved signal-to-noise of MDTs-CHA was obtained, which lead to more sensitivity and wider dynamic linear range for detecting exo-miRNA. To further confirm MDTs-CHA amplification process, the fluorescence signal of FAM to target miRNA was measured at 515 nm for 30 min (Fig. 1E). The H1 was modified by FAM and quencher in adjacent location, which would generate fluorescent signal in the presence of target miRNA. Upon addition of miRNA-1246, a time-dependent substantial increase in fluorescence was observed (black line). The maximum fluorescence signal of MDTs-CHA was obtained in 10 min, which is much faster than that of traditional CHA (red line), indicating that MDTs improve the efficiency of CHA greatly. On the other hand, the fluorescence enhancement of MDTs-CHA is 2.4 times higher than that of traditional CHA, which is in good agreement with the DPV results.

The high efficiency of MDTs-CHA was elucidated by using collision theory. The collision frequency tends to increase with reactants concentrations. The minimal volume of reaction system can be calculated based on the analytical formula V = 1/cN (where c represents hairpins concentration, and N represents Avogadro constant). When the concentration of H1 and H2 molecules in the solution was 25 nM, the volume of spherical droplets was 6.6×10^{-17} L with a radius of 251 nm (Fig. 1G). Under the circumstances of CHA, the distance between H1 and H2 was greatly shortened to be 5.78 nm (17 base pairs) because of MDTs. H1 interacted with H2 in the constrained sphere with radius of 5.78 nm, which elevated the local concentration to be 2.0 mM. Compared with CHA reacts in solution, the efficiency of MDTS-CHA is increased by a factor of 81,600. Therefore, H1 and H2 collided with each other more frequently and collision frequency was highly enhanced owing to the compact space provided by DNA tetrahedron, resulting in enhancement of reaction speed and efficiency.

3.3. Cascade amplification of MDTs-CHA

In order to get more powerful MDTs-CHA, the cascading of MDTs-CHA is studied further. As exhibited in Fig. 2A, programmable MDTs-CHA can be used for cascading amplification that can hold polynomial amplification of target exo-miRNA. But the background signals caused by initiator-independent reactions will be also amplified by cascade amplification, led to a serious reduced sensitivity. The sensitivity of the amplification strategy can be well reflected by signal to background ratio (S/B) (Zhang et al., 2015). Thus, to achieve better performance of MDTs-CHA, S/B of different layer MDTs-CHA is studied. The electrochemical measurements for different layer MDTs-CHA were 1.85, 6.51, 8.34 and 13.29 μA, with corresponding background signal of 0.27, 0.42, 0.78 and 1.86 μA (Fig. 2B), respectively. The two-layer MDTs-CHA holds the highest S/B by simple calculation (Fig. 2C). Moreover, the

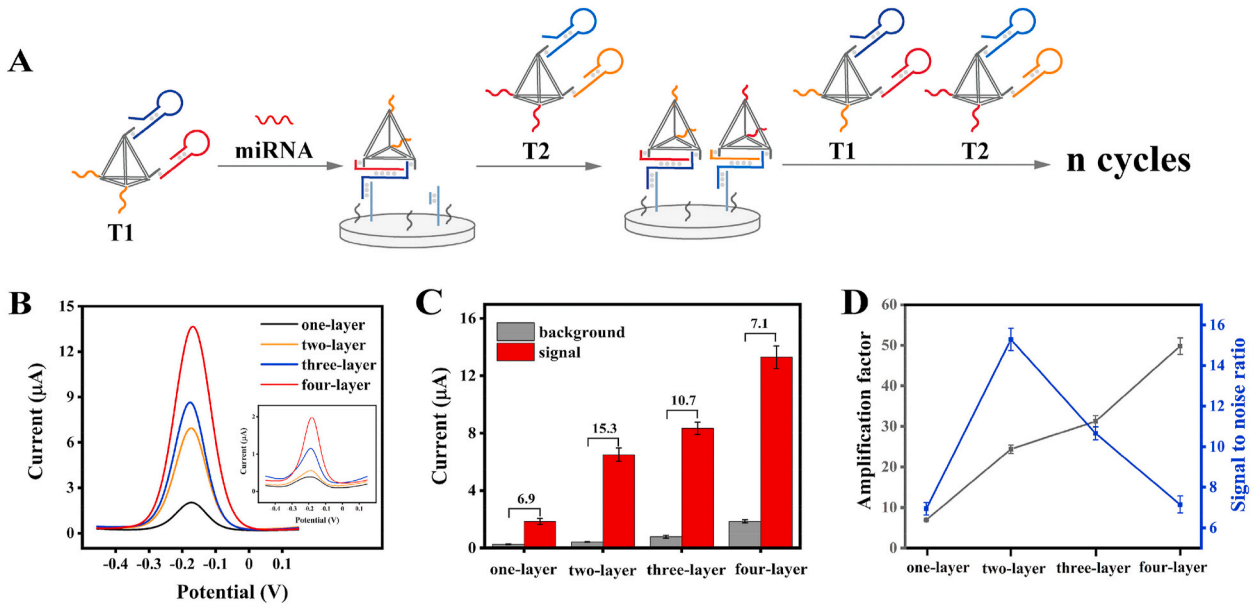

Fig. 2. (A) Schematic illustration of MDTs-CHA cascade amplification. (B) DPV signal for different layer of MDTs-CHA reactions. Inset shows the corresponding background signal of the MDTs-CHA. (C) S/B ratio for different layer of MDTs-CHA reactions. (D) Amplification factors and S/B ratios of different layer of MDTs-CHA reactions. The concentration of target was 100 pM.

amplification factors (AF, the ratio of electrochemical signal with and without MDTs-CHA) were achieved according to these experimental results. The AFs from one-layer to four-layer MDTs-CHA were calculated to be about 6.94, 24.39, 31.25 and 49.79, respectively, showing that the amplification factor increased slowly in the higher layer. These results demonstrated that the two-layer MDTs-CHA circuit obtains best S/B ratio, which ensured robust sensitivity and suitable operability.

3.4. Characterization of the biosensing strategy

The assembly steps of electrochemical biosensor on the electrode surface were characterized by EIS, SWV and CV. EIS is a technique that measures the impedance of a system varying with the alternating current frequency, and the diameter of semicircle on the curve is proportional to the electron transfer resistance (Ret). As depicted in Fig. 3A, the impedance curve of bare electrode was approximately of straight line, which indicated low Ret and good electronic conductivity (curve a). Subsequently, double-stranded capture probes were modified onto electrode interface via Au–S bond, resulting in aggregation of larger amounts of negatively charged DNA phosphate backbone. Thus, the $[Fe(CN)_6]^{3-/4-}$ molecules were rejected to approach the electrode interface and caused Ret increase (curve b). MCH molecules were next fabricated on surface of electrode, this biological macromolecules decreased background signals through blocking the non-specific binding sites. Besides, it also further impeded electron transfer from solution to surface because of large molecule dimension (curve c). In the presence of miR-1246, the MDTs-CHA reaction proceeded rapidly and the P strands exposed, and the DTs were captured by the capture probe on the electrode surface to enhance Ret greatly (curve d). Fig. 3B showed SWV characterization in different steps of assembly progress. The gradually decreased SWV results coincided with the increased impedance of EIS. CV results were also in good accordance with measurements of EIS (Fig. 3C). According to these results, the electrochemical biosensor based on MDTs-CHA was successfully established.

3.5. Analytical performance of the biosensor

To maximize the optimal analytical performance of the proposed biosensor, several parameters were studied in Fig. S2 and Fig. S3. The analytical performance included sensitivity, specificity, reproducibility and stability of this electrochemical platform was investigated under the optimal experimental conditions using DPV. The sensitivity of electrochemical biosensor using two-layer MDTs-CHA was first studied. As shown in Fig. 4A, the results exhibited that the current signal (I) increased gradually with the increasing of miRNA-1246 concentration ($C_{miR\text{-}1246}$) from 10 aM to 100 pM. There was a good linear correlation between the current signal and the logarithm of $C_{miR\text{-}1246}$ (Fig. 4B), fitted as $I = 0.814\ lgC_{miR\text{-}1246} + 14.391$ with correlation coefficient of 0.993.

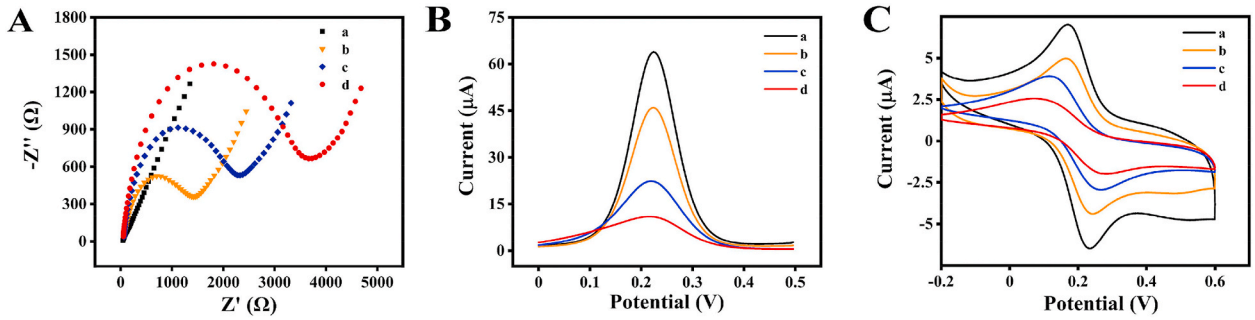

Fig. 3. EIS (A), SWV (B) and CV (C) in 0.4 M KCl containing 0.5 mM $Fe(CN)_6^{3-/4-}$ at bare electrode (a); the electrode modified by capture DNA (b); the modifed electrode surface after MCH immobilization (c); MDTs-CHA captured by modified electrode with the addition of target miRNA (d).

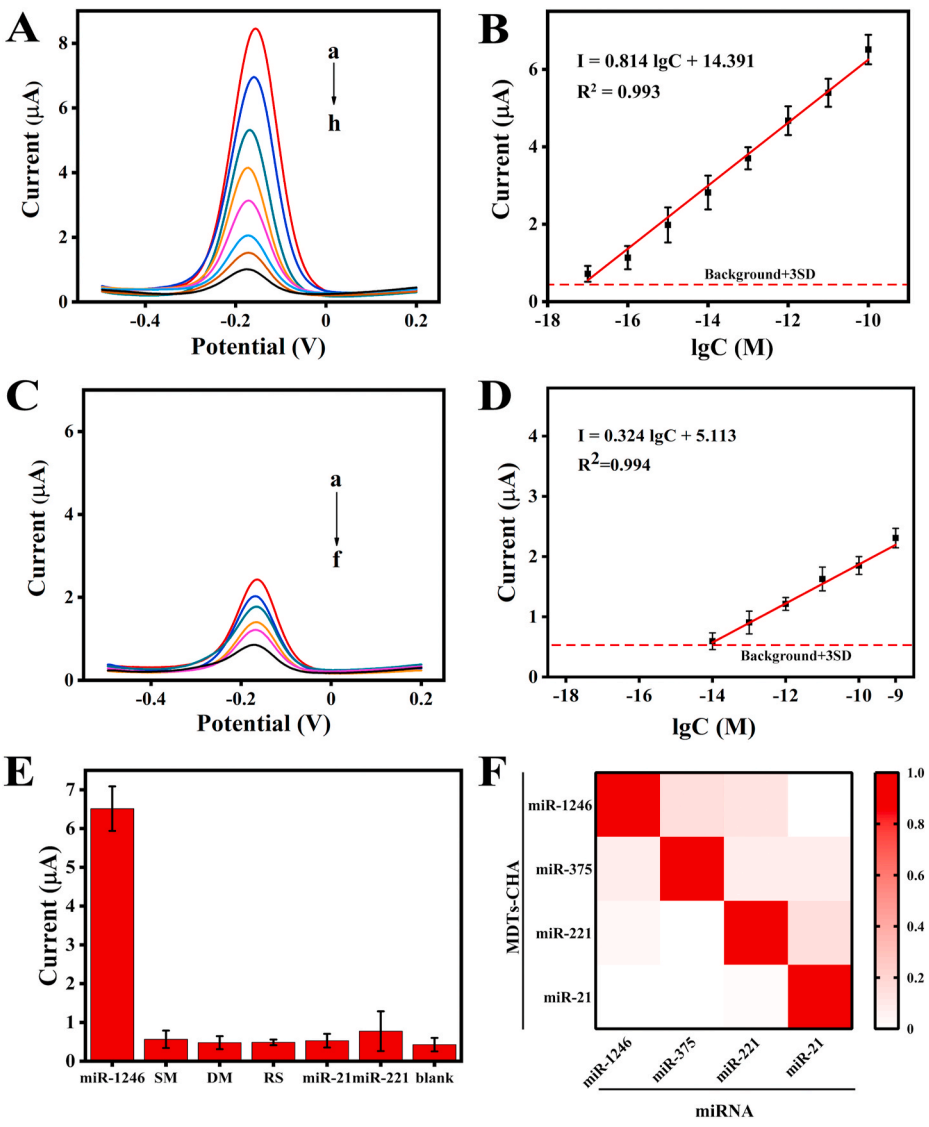

Fig. 4. (A) DPV responses and (B) the corresponding calibration curve to 100, 10, 1, 0.1, 0.01, 0.001, 0.0001 and 0.00001 pM of target exo-miRNA (from a to h) using two-layer MDTs-CHA. (C) DPV responses and (D) the corresponding calibration curve to 1000, 100, 10, 1, 0.1 and 0.01 pM of target exo-miRNA using typical DTs-CHA amplification. (E) DPV results respectively respond to the target exo-miR-1246 and five interferences with a concentration of 100 pM. (F) Heat map analysis of the orthogonal identification of four homologous miRNAs. The error bars represent the standard deviations (n = 3).

The limit of detection (LOD) was 7.2 aM based on 3SD corresponding to the blank tests. To highlight the advantages of designed MDTs-CHA, the measurements were implemented by typical DTs-CHA under the same condition. The linear range from 10 fM to 100 pM was obtained with LOD of 7.8 fM (Fig. 4C and D). The LOD of MDTs-CHA was 1083-fold lower than typical DTs-CHA, and 84,930-fold lower than that of CHA (Fig. S4), which demonstrated the powerful signal amplification of proposed MDTs-CHA amplification.

The specificity of the proposed biosensor was studied by measuring different groups of miRNA, including single-base mismatch miRNA (SM), two-bases mismatched miRNA (DM), random sequence (RS), and some high homologous miRNA (miRNA-21, miRNA-221) (Zhang et al., 2020a). As shown in Fig. 4E, the DPV responses from target miRNA-1246 were at least 20 times greater than that of mismatched miRNA and homologous miRNA, demonstrating high selectivity of the proposed biosensor. To better illustrate the specificity of MDTs-CHA assay, we evaluated the cross-responses of MDTs-CHA toward four miRNAs by using orthogonal identification. The results are shown in Fig. 4F. Compared to target miRNA, MDTs-CHA only produced negligible signal when responded to non-target homologous miRNAs. To study the reproducibility of the biosensor, the samples contained 100 fM target miRNA were tested in five different batches. The variable coefficient of the results was around 3.9%, demonstrating an admirable reproducibility of the proposed biosensor. Meanwhile, to assess the stability of this biosensor, the DPV was measured at intervals of two days with the addition of 10 pM miRNA-1246 during 10 days. As seen in Fig. S5, the DPV signals were maintained to with 92.62% of the initial measurement.

In general, compared to other biosensor for the detection of exo-miRNA (Table S2), the developed platform based two-layer MDTs-CHA has the better sensitivity and specificity with suitable process. Although SERS based methods have higher sensitivity, their complex operation and expensive facility may limit their clinical applications. In our work, the electrochemical biosensor with advantages included low cost, rapid detection, and easy to use will promote the advance of the point-of-care testing.

3.6. Real sample analysis

Before detection of exo-miR-1246, standard ultracentrifugation method was used to obtain exosomes from breast cancer MDA-MB-231 cells, and the acquired exosomes were characterized. TEM images exhibited a group of round and partially collapsed structures with diameters of 110 nm, which is consistent with the previous reported (Gong et al., 2019) (Fig. S6A). A homogeneous population ranging from 66 to 216 nm with a peak at 104 nm was showed by NTA (Fig. S6B). Several

exosome specific markers (CD9, CD63, and CD81) and membrane proteins TSG101 were proven by Western blotting (Fig. S6C). These results demonstrated that the exosomes derived from MDA-MB-231 cells were obtained successfully.

Subsequently, the exosomes derived from three cell lines (MDA-MB-231 cell line; MCF-7 cell line; and 16HBE cell line) were isolated to extract total RNA. The developed biosensor and RT-PCR were used to analysis the expression level of exo-miR-1246. As shown in Fig. S7, the DPV signal of exo-miRNA-1246 derived from MDA-MB-231 cell was 2.3 and 3.4 times that of derived from MCF-7 and 16HBE, respectively. The identical results were obtained from standard RT-PCR (Fig. S8), which further validated the feasibility of the proposed electrochemical biosensor in clinical application.

To further study the clinical use of proposed platform, we studied a breast cancer patient cohort (n = 30; that is 9 for healthy donors, 10 for breast cancer with stage I-IIA, 11 for breast cancer with stage IIB-IV) (Table S3). MDTs-CHA contained different target-initiated CHAs were used to analysis a panel of four breast cancer-associated exo-miRNAs (miR-1246, miR-221, miR-375, and miR-21) (Li et al., 2020b; Wu et al., 2021; Zhao et al., 2020b). The heat map in Fig. 5A summarized the normalized signals of four exo-miRNAs, which reflected the expression level by colour intensity. As shown in Fig. 5B–E, the Mann–Whitney *U* test was used for DPV measurements analysis. These results demonstrated that exo-miR-375 was the best marker for predicting malignant breast cancer ($p < 0.05$), which were consistent with previous research (Zhao et al., 2020a). The diagnostic efficacy was also analyzed further by ROC curve. As shown in Fig. 5F–G and Fig. S9, the combination of exo-miR-375, exo-miR-1246, exo-miR-221, and exo-miR-21 showed a higher accuracy (AUC: 0.989, 95% CI: 0.962 to 1.000) than a single exo-miRNA for identifying patient with breast cancer from HD. Of particular interest was that combination of exo-miRNA showed a sensitivity of 80%, a specificity of 80% and an AUC of 0.755 for early detection of breast cancer (stages I-IIA, Fig. 5H and Figs. S10 and S11). In conclusion, the proposed platform provides a viable alternative for clinical application.

4. Conclusions

In summary, a label-free and rapid electrochemical platform for detecting exo-miRNAs was proposed using multifunctional DNA tetrahedron assisted catalytic hairpin assembly. The MDTs acts as a carrier not only used for accelerating and cascading the CHA amplification, but also processing amplified electrochemical signal by loading Ruhex, which improves the amplification efficiency greatly. Benefiting from the two-layer MDTs-CHA amplification, this biosensor can detect the exo-miRNA down to 7.2 aM in 30 min. The outstanding specificity,

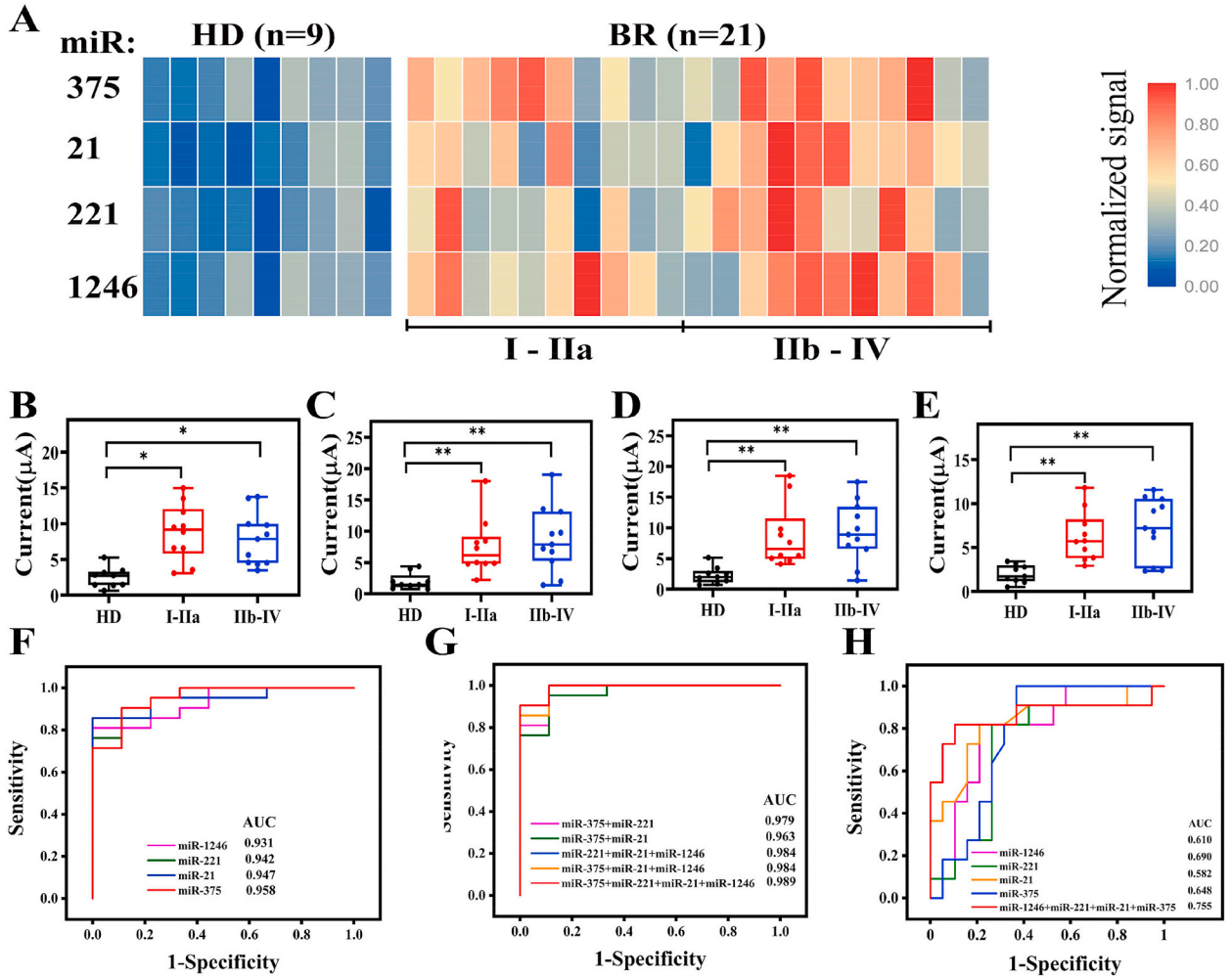

Fig. 5. Profiling four exo-miRNAs in breast tumor cohort by the developed biosensor. (A) Heat map of exo-miRNAs profiling in the HD (n = 9) and patient groups with breast cancer in stage I-IIA (n = 10), stage IIB-IV (n = 11). The intensity is based on single measurement by the biosensor. DPV signal for exo-miRNAs (B) exo-miR-375, (C) exo-miR-21, (D) exo-miR-221 and (E) exo-miR-1246 profiling in samples from HD, patient with breast cancer in stage I-IIA and stage IIB-IV (*, $p < 0.05$; **, $p < 0.01$). ROC curve of single exo-miRNA (F) and combined multiple exo-miRNA (G) for identifying patients with breast tumors. (G) ROC curve of exo-miRNA for diagnosing breast cancer in early stages (I-IIA).

stability and reproducibility of this platform possess some intrinsic features including easy to use, rapid, and high portability. Moreover, Applying proposed platform to breast cancer patients demonstrated that profiling of exo-miRNAs was a promising way for early detection of cancer. Besides, standard procedure for clinical sample exo-miRNA analysis was established, which greatly improved the repeatability and comparability. Considering the feasibility of this method, MDTs-CHA can be adopted for detecting multiple exosomal biomarkers in clinical applications.

CRediT authorship contribution statement

Ye Zhang: Experimentation, Conceptualization, Writing – review & editing, Writing. **Xiaohe Zhang:** Experimentation, Writing – review & editing, Writing. **Bo Situ:** Experimentation. **Yuan Wu:** Experimentation. **Shihua Luo:** Experimentation. **Lei Zheng:** Conceptualization, Writing – review & editing, Writing, Editing. **Yurong Qiu:** Conceptualization, Writing – review & editing, Writing, Editing.

Declaration of competing interest

The authors declare that they have no known competing financial interests or personal relationships that could have appeared to influence the work reported in this paper.

Acknowledgements

This study was supported by the National Natural Science Foundation of China (81802114 and 81871712).

Appendix A. Supplementary data

Supplementary data to this article can be found online at https://doi.org/10.1016/j.bios.2021.113205.

References

Chen, J., Wu, Y., Fu, C., Cao, H., Tan, X., Shi, W., Wu, Z., 2019. Biosens. Bioelectron. 143, 1116–1119.
Chu, Y., Deng, A.P., 2019. Anal. Chem. 91, 3619–3627.
Gao, X., Li, S., Ding, F., Fan, H., Shi, L., Zhu, L., Li, J., Feng, J., Zhu, X., Zhang, C., 2019. Angew Chem. Int. Ed. Engl. 58, 8719–8723.
Gong, C., Tian, J., Wang, Z., Gao, Y., Wu, X., Ding, X., Qiang, L., Li, G., Han, Z., Yuan, Y., Gao, S., 2019. J. Nanobiotechnol. 17, 93.
Huang, Q., Ma, P.-Q., Li, H.-D., Yin, B.-C., Ye, B.-C., 2020. ACS Appl. Bio Mater. 3, 2861–2866.
Imjeti, N.S., Menck, K., 2017. Proc. Natl. Acad. Sci. U. S. A. 114, 12495–12500.
Kalluri, R., 2016. J. Clin. Invest. 126, 1208–1215.
Kalluri, R., LeBleu, V.S., 2020. Science 367, eaau6977.
Lee, J.U., Kim, W.H., Lee, H.S., Park, K.H., Sim, S.J., 2019. Small 15, e1804968.
Li, J., Liu, J., Bi, Y., Sun, M., Bai, J., Zhou, M., 2020a. Anal. Chim. Acta 1105, 87–94.
Li, N., Shen, F., Cai, Z., Pan, W., Yin, Y., Deng, X., Zhang, X., Machuki, J.O., Yu, Y., Yang, D., Yang, Y., Guan, M., Gao, F., 2020b. Small 16, e2005511.
Li, X., Li, X., Li, D., Zhao, M., Wu, H., Shen, B., Liu, P., Ding, S., 2020c. Biosens. Bioelectron. 168, 112554.
Li, Y., Han, H., Wu, Y., Yu, C., Ren, C., Zhang, X., 2019. Biosens. Bioelectron. 142, 111543.
Liao, X., Zhang, C., Machuki, J.O., Wen, X., Chen, D., Tang, Q., Gao, F., 2021. Talanta 226, 122058.
Lin, M., Wen, Y., Li, L., Pei, H., Liu, G., Song, H., Zuo, X., Fan, C., Huang, Q., 2014. Anal. Chem. 86, 2285–2288.
Liu, L., Lu, H., Shi, R., Peng, X.X., Xiang, Q., Wang, B., Wan, Q.Q., Sun, Y., Yang, F., 2019. ACS Appl. Mater. Interfaces 91, 13198–13205.
Liu, P., Qian, X., Li, X., Fan, L., Li, X., Cui, D., Yan, Y., 2020. ACS Appl. Mater. Interfaces 12, 45648–45656.
Miao, P., Tang, Y., 2020. Anal. Chem. 92, 12026–12032.
Miti, A., Thamm, S., Müller, P., Csáki, A., Fritzsche, W., Zuccheri, G., 2020. Biosens. Bioelectron. 167, 112465.
Ning, Z., Zheng, Y., Pan, D., Zhang, Y., Shen, Y., 2020. Biosens. Bioelectron. 150, 111945.
Ozhalici-Unal, H., Armitage, B.A., 2009. ACS Nano 3, 425–433.
Pang, Y., Wang, C., Lu, L., Wang, C., Sun, Z., Xiao, R., 2019. Biosens. Bioelectron. 130, 204–213.
Ratajczak, J., Miekus, K., Kucia, M., Zhang, J., Reca, R., Dvorak, P., Ratajczak, M.Z., 2006. Leukemia 20, 847–856.
Reese, M., Flammang, I., Yang, Z., Dhayat, S.A., 2020. Cancers (Basel) 12.
Shen, F., Zhang, C., Cai, Z., Wang, J., Zhang, X., Machuki, J.O., Cui, L., Li, S., Gao, F., 2020. ACS Appl Mater Interfaces.
Tang, X., Wang, Y., Zhou, L., Zhang, W., Yang, S., Yu, L., Zhao, S., Chang, K., Chen, M., 2020. Mikrochim. Acta 187, 172.
Tavallaie, R., McCarroll, J., Le Grand, M., Ariotti, N., Schuhmann, W., 2018. Nat. Nanotechnol. 13, 1066–1071.
Théry, C., Zitvogel, L., Amigorena, S., 2002. Nat. Rev. Immunol. 2, 569–579.
Valadi, H., Ekström, K., Bossios, A., Sjöstrand, M., Lee, J.J., Lötvall, J.O., 2007. Nat. Cell Biol. 9, 654–659.
Wang, D., Chai, Y., 2020. ACS Appl. Mater. Interfaces 12, 2871–2877.
Wang, J., Wang, D.X., Ma, J.Y., Wang, Y.X., Kong, D.M., 2019. Chem. Sci. 10, 9758–9767.
Wang, R., Zhao, X., Chen, X., Qiu, X., Qing, G., Zhang, H., Zhang, L., Hu, X., He, Z., Zhong, D., Wang, Y., Luo, Y., 2020. Anal. Chem. 92, 2176–2185.
Wu, Y., Zhang, Y., Zhang, X., Luo, S., Yan, X., Qiu, Y., Zheng, L., Li, L., 2021. Biosens. Bioelectron. 177, 112962.
Yan, W., Wu, X., Zhou, W., Fong, M.Y., Cao, M., Liu, J., Liu, X., Chen, C.H., Fadare, O., Pizzo, D.P., Wu, J., Liu, L., Liu, X., Chin, A.R., Ren, X., Chen, Y., Locasale, J.W., 2018. Nat. Cell Biol. 20, 597–609.
Zeng, Z., Li, Y., Pan, Y., Lan, X., Song, F., Sun, J., Zhou, K., Liu, X., Ren, X., Wang, F., Hu, J., Zhu, X., Yang, W., Liao, W., Li, G., Ding, Y., Liang, L., 2018. Nat. Commun. 9, 5395.
Zhang, G.J., Wang, L.L., Chen, W.Q., Wang, Y.R., Zeng, L.P., Chen, T.T., Chen, G.Y., Chen, J.H., 2020a. Anal. Chem. 169, 112555.
Zhang, W., Xu, H., Zhao, X., Tang, X., Yang, S., Yu, L., Zhao, S., Chang, K., Chen, M., 2020b. Anal. Chim. Acta 1122, 39–47.
Zhang, Y., Luo, S., Situ, B., Chai, Z., Li, B., Liu, J., Zheng, L., 2018. Biosens. Bioelectron. 102, 568–573.
Zhang, Y., Yan, Y., Chen, W., Cheng, W., Li, S., Ding, X., Li, D., Wang, H., Ju, H., Ding, S., 2015. Biosens. Bioelectron. 68, 343–349.
Zhao, J., Liu, C., Li, Y., Ma, Y., Deng, J., Li, L., 2020a. J. Am. Chem. Soc. 142, 4996–5001.
Zhao, J., Liu, C., Li, Y., Ma, Y., Deng, J., Li, L., Sun, J., 2020b. J. Am. Chem. Soc. 142, 4996–5001.
Zhu, L., Zhang, M., Ye, J., Yan, M., Zhu, Q., Huang, J., Yang, X., 2020. Anal. Chem. 92, 8614–8622.